

CONSTRAINED-MOTION DRILLING DYNAMOMETER DESIGN AND EVALUATION

Ross Zamoski¹, Christoph Ramsauer², Christoph Habersohn², Friedrich Bleicher², and Tony Schmitz^{1,3}

¹Department of Mechanical, Aerospace, and Biomedical Engineering
University of Tennessee, Knoxville
Knoxville, TN, 37996, USA

²Institute for Manufacturing Engineering and Photonic Technologies
Technical University of Vienna
1030 Vienna, Austria

³Manufacturing Demonstration Facility
Oak Ridge National Laboratory
Oak Ridge, TN, 37830, USA

ABSTRACT

This paper describes the design and evaluation of a constrained-motion drilling dynamometer for torque and thrust force measurement. A two degree of freedom design, based on constrained-motion flexure-based kinematics is implemented. The drilling torque and thrust force are inferred from displacement measurements using a dual-magnet Hall effect sensor configuration. Rotationally compliant flexure elements are integrated into the design to infer the torque from the rotary motion. Translationally compliant flexure elements are integrated into the design to infer the thrust force from the linear motion. Two sensors are implemented for each direction to reject undesired structural dynamics. The measured rotational and translational motions are combined with the dynamometer stiffness values to derive the drilling torque and thrust force. To validate the constrained-motion drilling dynamometer (CMDD), experiments were performed and compared to the measurement performance of a commercially available, piezoelectric-based drilling dynamometer.

INTRODUCTION

Force measurement in drilling operations is key for improvements in industrial automation and control. However, in drilling it is difficult to measure cutting forces at their origin (i.e., the cutting edge-chip interface). This has led to the development of indirect force measurement methods which measure the displacement or strain of a component within the machine tool's structure to infer the cutting force. Solutions using piezoelectric force transducers have become common but are often limited by their structural dynamics. Other methods of force measurement have been developed and are highlighted in [1],

[2], [3]. Here, the proposed solution differs from previous efforts because it combines a constrained-motion design with low-cost Hall effect sensors and a dual magnet arrangement. This solution can provide simultaneous drilling torque and thrust force measurements with the required bandwidth.

DYNAMOMETER DESIGN

A flexure-based design is implemented, where the applied drilling torque is determined from the rotational displacement of the dynamometer's workpiece mounting stage and the drilling thrust force is determined from the translational displacement of the dynamometer's platform. The workpiece mounting stage is radially supported by rotationally compliant flexure elements (spokes), while the platform is vertically supported by translationally compliant flexure elements (leaves); see FIGURE 1.

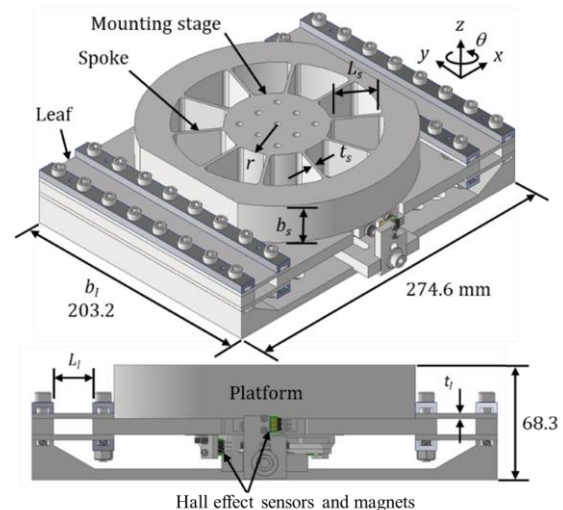


FIGURE 1. CMDD design

Both sets of flexure elements were fabricated from 6061-T6 aluminum (elastic modulus, E , of 69 GPa and yield strength, σ_y , of 276 MPa). A hub-spoke flexure element structure is integrated into the CMDD platform to provide a well-defined, repeatable rotation that is proportional to the applied drilling torque. The rotational stiffness, K_θ , is given by Eq. 1, where N_s is the number of spokes, L_s is the spoke length in the radial direction, b_s is the spoke width, t_s is the spoke thickness, and r is the mounting stage radius [4].

$$K_\theta = \frac{N_s E b_s t_s^3}{3} \left(\frac{1}{L_s} + \frac{3r}{L_s^2} + \frac{3r^2}{L_s^3} \right) \quad (1)$$

Leaf-type flexure elements are clamped in an H-bar arrangement to dynamometer's platform to preferentially allow motion in the compliant (vertical) direction, while restricting motion in all other directions. The translational stiffness, K_z , is given by Eq. 2, where L_l is the leaf length, b_l is the leaf width, t_l is the leaf thickness, and N_l is the number of flexure elements [5].

$$K_z = N_l E b_l \left(\frac{t_l}{L_l} \right)^3 \quad (2)$$

Since both stiffnesses are largely dependent on the flexure thickness and length, a contour plot is generated to depict lines of constant stiffness as a function of the thickness and length; see FIGURE 2. The plot also includes red circles to highlight the selected design parameters. A summary of the selected flexure geometry and the corresponding stiffnesses is outlined in TABLE 1.

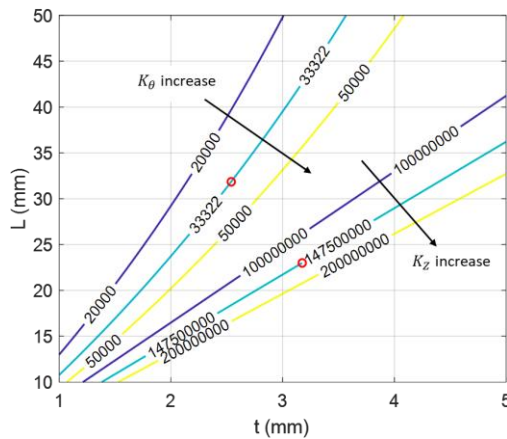


FIGURE 2. Lines of constant stiffness based on spoke and leaf thickness (t) and length (L).

TABLE 1. CMDD design dimensions and stiffness values.

Mounting stage				
L_s (mm)	b_s (mm)	t_s (mm)	r (mm)	K_θ (Nm/rad)
31.85	31.75	2.540	38.10	3.33×10^4
Platform				
L_l (mm)	b_l (mm)	t_l (mm)		K_z (N/m)
23.00	203.2	3.175		1.48×10^8

Finite element analysis, FEA (ANSYS Workbench), was implemented for further stiffness predictions. To determine the rotational stiffness, a 1 Nm moment was applied to the central axis of the mounting stage and the rotation was recorded at the outer diameter. The applied moment was divided by the recorded rotation to obtain the rotational stiffness. To evaluate the translational stiffness, a 1 N vertical force was applied to the top center of the mounting stage and the displacement of the stage was recorded. The mounting stage was modeled as rigid, so that its compliance would not contribute to the overall deflection; see TABLE 2 for the stiffness results. In practice, the compliance of the mounting stage does contribute to the system's translational stiffness. When including the deflection of the mounting stage, the equivalent translational stiffness predicted by FEA was $K_{z,eq} = 6.75 \times 10^7$ N/m.

TABLE 2. Comparison of analytical and FEA stiffness values (rigid platform).

K_θ (Nm/rad)		
Analytical	FEA	Percent difference (%)
3.33×10^4	3.30×10^4	-1.04
K_z (N/m)		
1.48×10^8	1.63×10^8	9.20

Modal finite element simulations were performed to ensure sufficient frequency separation of the vibration modes and to approximate each motion as a single degree of freedom, see TABLE 3. The first mode natural frequency (platform vertical displacement) was found to be closely spaced with the second mode natural frequency (platform tilting). To minimize the effect of the second mode in deflection measurement, two Hall effect sensors were positioned such that averaging their responses negates the influence of the second mode. The third mode (mounting stage rotation)

was sufficiently separated from the other modes, allowing the rotational dynamics to be approximated with a single degree of freedom. Two Hall effect sensors were also used to measure the rotational response, with their measurements averaged.

TABLE 3. CMDD modes of vibration.

Natural freq.	Description
892 Hz	Platform vertical displacement (intended)
962 Hz	Platform out-of-plane tilt
1448 Hz	Mounting stage rotation (intended)
1605 Hz	Platform out-of-plane tilt
2558 Hz	Platform twist

SENSOR SELECTION

A key component of the CMDD is that the measurement transducers are cost-effective, compact, and reliable. A bipolar Hall effect sensor (Texas Instruments DRV5055A2QDBZR) was selected to meet these design requirements. A high sensitivity in linear response displacement measurement can be achieved by using two magnets (N52 gold-plated neodymium disc magnets), fixed next to each other with opposite polarities facing the bipolar sensor. This sensor-magnet configuration was evaluated using a linear air bearing positioning stage (Aerotech ABL 10100-LT) with a positioning uncertainty of $\pm 5 \mu\text{m}$ and resolution of 2.5 nm. A calibration procedure was performed to determine the relationship between the sensor's output voltage and the magnet position. As the magnets traversed past the sensing element in the dual magnet with opposite pole configuration, the response varied linearly from the low to high voltage saturation levels. This sensor-magnet combination had a linear range of 250 μm and a sensitivity of 36.8 $\mu\text{m}/\text{V}$ (0.2 mm sensor-magnet air gap); see FIGURE 3.

With the characteristics of the sensor, the measureable drilling torque and thrust force are calculated. The measureable torque, T , is calculated by multiplying the rotational stiffness by the rotation, θ , as shown in Eq. 3. Here, the small angle approximation is used to calculate the rotation by dividing the mounting stage displacement, x , by the sensor's distance from the center of the stage, d . The mounting stage

displacement is the product of the sensor's sensitivity, S , and output voltage, V . The measureable thrust force, is determined by finding the product of the platform displacement, z , and the sensor's sensitivity and output voltage, as shown in Eq 4. It was determined that the value for d was 51.7 mm and the sensor noise level was 0.005 V. The maximum and minimum measureable torque values are then determined to be 166.6 Nm and 0.1 Nm. The maximum and minimum measureable thrust forces are 16,875 N and 12.4 N.

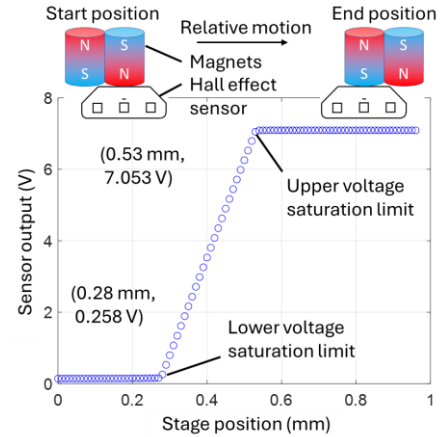


FIGURE 3. Calibration curve for selected sensor-magnet combination.

$$T = K_{\theta} \theta = K_{\theta} \frac{x}{d} = K_{\theta} \frac{SV}{d} \quad (3)$$

$$F = K_{z,eq} z = K_{z,eq} SV \quad (4)$$

INITIAL TESTING

A prototype dynamometer was used to validate the predicted rotational and translational stiffnesses through mass loading experiments. The rotational stiffness was measured by fixing the CMDD to a machining center table, hanging a known mass at a selected radius to apply a torque, and using the Hall effect sensor measured rotation to calculate the stiffness; see FIGURE 4. Five masses (1.030 kg to 4.688 kg) were selected and suspended from each hole in the mounting stage. The holes in the mounting stage were organized in three rows (1-3) and three columns (A-C) to enable measurements at multiple locations. For each hole-mass combination, the the voltage change measured by the Hall effect sensors was converted to rotation using the sensor's sensitivity and radial distance. The torque was determined by multiplying the applied force by the radial

distance. Two stiffness values were obtained by dividing the applied torque by the measured rotation; these stiffness values were averaged to obtain the final stiffness. The overall average from all measurements was 3.17×10^4 Nm/rad with a standard deviation of 935 Nm/rad, which is 4.8% lower than the analytical solution and 3.8% lower than the FEA solution in TABLE 2.

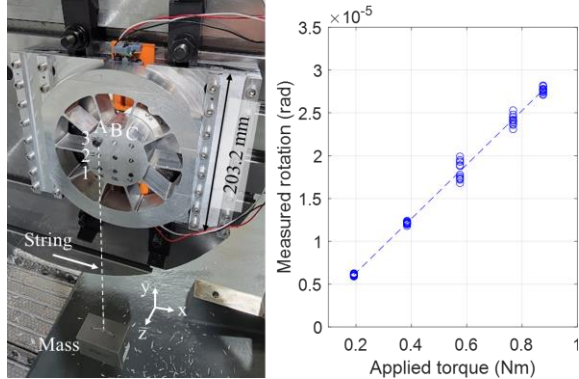


FIGURE 4. Static rotational stiffness experimental setup with 3-A application location (left). Calibration data and least square fit (right).

Before conducting drilling experiments, thermoplastic polyurethane (TPU) damping inserts were fabricated through fused filament fabrication. The inserts were placed between the spokes to increase damping and provide shielding for the sensors. The experiment to validate the rotational stiffness was repeated to examine how the inclusion of the inserts affected the stiffness. Here, the average value from all measurements was 3.36×10^4 Nm/rad (5.9% larger than without the damping inserts) with a standard deviation of 820 Nm/rad. To validate the translational stiffness, the stiffness was measured by placing a known mass on the center of the mounting stage and measuring the platform deflection with the Hall effect sensors. Eddy current displacement sensors (Micro-epsilon EPU05-C3-A/M) were also deployed for comparison. Six masses (3.069 kg to 10.388 kg) were used to apply the thrust force. The measured displacements were averaged and plotted against the applied force. The slope of the best fit line was 1.93×10^{-8} m/N, which corresponds to a translational stiffness of 5.18×10^7 N/m (26.3% less than compliant platform FEA solution).

DRILLING EXPERIMENTS

Drilling tests were conducted to compare the measurement results of the CMDD to a commercially available, rotating dynamometer

(Kistler 9170A1312). Two workpiece materials (6060 aluminum and DIN EN 1.4301 stainless steel) were selected and the samples were bolted to the CMDD. Blind holes were drilled with 8 mm and 12 mm diameter, two flute, solid carbide, TiAlN coated drills with 140 deg point angles (Kennametal 1913487 and 1913502). The drilling parameters are presented in TABLE 4. A DMG-Mori DMU 75 monoBLOCK five-axis CNC machining center was used for the experiments. Tests were performed without flood coolant, but a Stoddard solvent (WD-40) was applied to the workpiece surface prior to drilling to prevent the chips from adhering to the tool. A center drilling operation was performed prior to the drilling tests; see the setup in FIGURE 5.

TABLE 4. Drilling parameters.

Material	6060 aluminum		1.4301 stainless steel	
	Dia. (mm)	8	12	8
Feed (mm/min)	573, 716, 860	572, 764	143, 191	127, 170
Spindle speed (rpm)	3,581	2,387	1,592	1,061
Depth (mm)	12	18	12	12

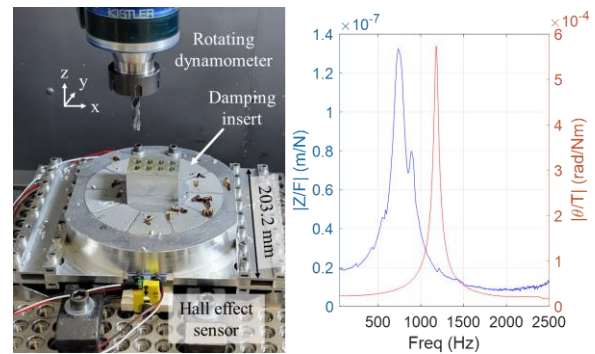


FIGURE 5. Drilling setup on DMG-Mori DMU 75 with an aluminum sample bolted to the CMDD. The drill is clamped in the rotating dynamometer (left). Measured frequency response functions of the CMDD (right).

To evaluate repeatability, three holes were drilled for each parameter combination. The drilling torque and thrust force were determined from the mean values of the steady-state portion from each test; see FIGURE 6. For a given parameter set, the three mean values were averaged to report the drilling torque and thrust force. To represent the noise in the drilling torque and thrust force signals, the standard deviation from

each steady state region was calculated. The propagation of uncertainty formula was used to combine the standard deviations and find the combined standard uncertainty in the drilling torque and thrust force.

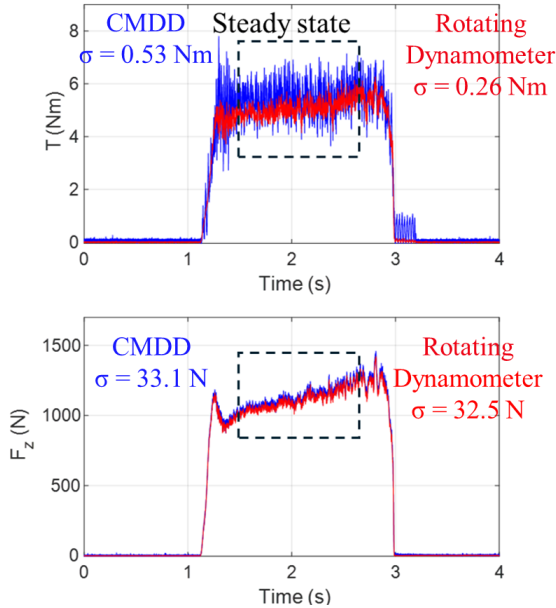


FIGURE 6. Time domain torque (top) and thrust force (bottom) signals.

Comparisons of the measured drilling torque and thrust force values are displayed in FIGURE 7 and FIGURE 8. It is observed that the CMDD drilling torque demonstrates overlapping error bars with the rotating dynamometer and mean values that differ by 8.2% or less. The CMDD thrust force again demonstrates overlapping error bars with the rotating dynamometer and the maximum difference is 7.9%.

CONCLUSIONS

The design, development, and testing of a constrained-motion drilling dynamometer (CMDD) for simultaneous drilling torque and thrust force measurement was outlined. The two degree of freedom design enabled the CMDD to infer the applied drilling torque from measurements of the workpiece mounting stage rotational displacement, while the thrust force was inferred from measurements of the dynamometer's platform displacement. Rotational and translational flexure elements were implemented to provide the desired motion. Displacement measurements were performed using two pairs of dual magnet-Hall effect sensors. The opposite pole arrangement of the

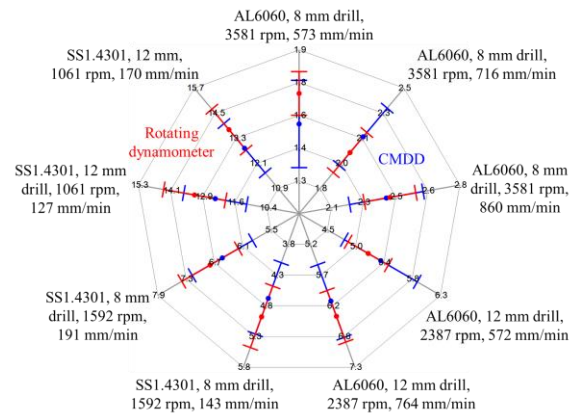


FIGURE 7. Radar chart comparing the CMDD and rotating dynamometer drilling torque (Nm). Each radial axis represents a combination of drilling parameters and the error bars represent two standard deviations (95% confidence interval). Note the change in scale along each axis.

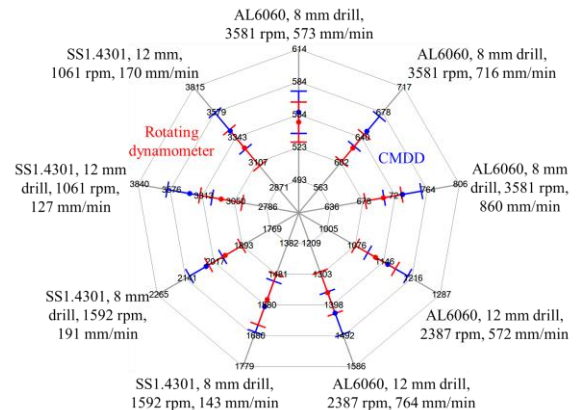


FIGURE 8. CMDD and rotating dynamometer thrust force (N) comparison.

magnets provided a linear response over the full sensor range, while the sensor pairs enabled the rejection of undesired structural dynamics. Torque and thrust force measurement results were presented for both the CMDD and a commercially available rotating dynamometer. A comparison of the two dynamometers from multiple drilling conditions showed a maximum percent difference of 8.2% for torque and 7.9% for thrust force; overlapping error bars were observed in all cases. Future work will include additional calibration studies (e.g., the CMDD consistently measured higher thrust force) and design refinements to reduce the CMDD footprint. A study of application use cases, such as tool wear monitoring, will also be conducted.

ACKNOWLEDGEMENTS

The authors acknowledge financial support from the Austrian Marshall Plan Foundation and equipment support from the Machine Tool Technologies Research Foundation (MTTRF).

REFERENCES

- [1] Ramsauer, C., Leitner, D., Habersohn, C., Schmitz, T. L., Yamazaki, K., Bleicher, F. (2023). Flexure-based dynamometer for vector-valued milling force measurement. *Journal of Machine Engineering*. <https://doi.org/10.36897/jme/161234>
- [2] Sousa, V. F. C., Silva, F. J. G., Fecheira, J. S., Lopes, H. M., Martinho, R. P., Casais, R. B., & Ferreira, L. P. (2020). Cutting forces assessment in cnc machining processes: A criticalreview review. *Sensors (Switzerland)*, 20(16), 1–26. <https://doi.org/10.3390/s20164536>
- [3] Totis, G., Adams, O., Sortino, M., Veselovac, D., & Klocke, F. (2014). Development of an innovative plate dynamometer for advanced milling and drilling applications. *Measurement: Journal of the International Measurement Confederation*, 49(1), 164–181. <https://doi.org/10.1016/j.measurement.2013.11.049>
- [4] Tsetserukou, D., Tadakuma, R., Kajimoto, H. and Tachi, S., 2006, May. Optical torque sensors for implementation of local impedance control of the arm of humanoid robot. In *Proceedings 2006 IEEE International Conference on Robotics and Automation, 2006. ICRA 2006.* (1674-1679). IEEE.
- [5] Smith, S.T., 2000. *Flexures: Elements of Elastic Mechanisms*. CRC Press.